# Highly Efficient Cobalt-Modified Hopcalite Catalyst Prepared through the Crednerite-Spinel Transformation

[1]Svintsitskiy D.A., [1]Kvasova E.S., [1]Kardash T.Yu., [1,2]Sokovikov N.A., [1]Stonkus O.A., [1]Boronin A.I.

1 – Boreskov Institute of Catalysis, Pr. Lavrentieva 5, 630090, Novosibirsk, Russia

2 – Novosibirsk State University, St. Pirogova 2, 630090, Novosibirsk, Russia

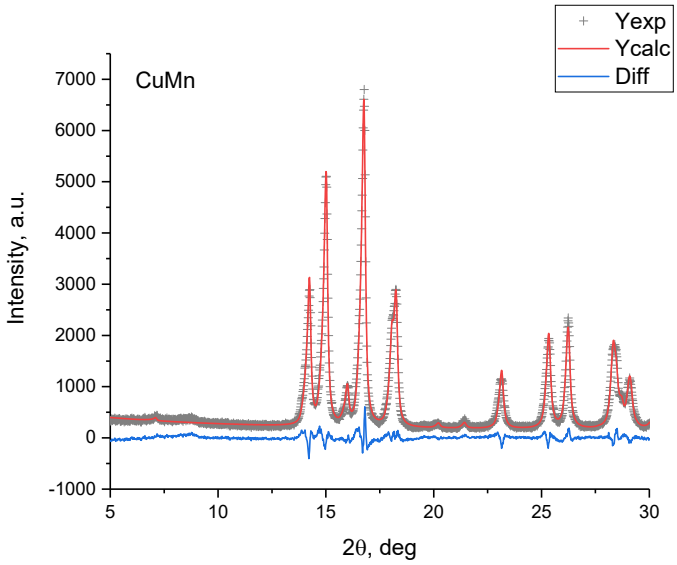


***Figure S1. Both experimental (+) and simulated (red line) X-ray patterns for as-prepared CuMn sample. Simulation was performed using the Rietveld method. Blue line corresponds to difference curve. The obtained value of $R_{wp}$ is close to 7.8%.***

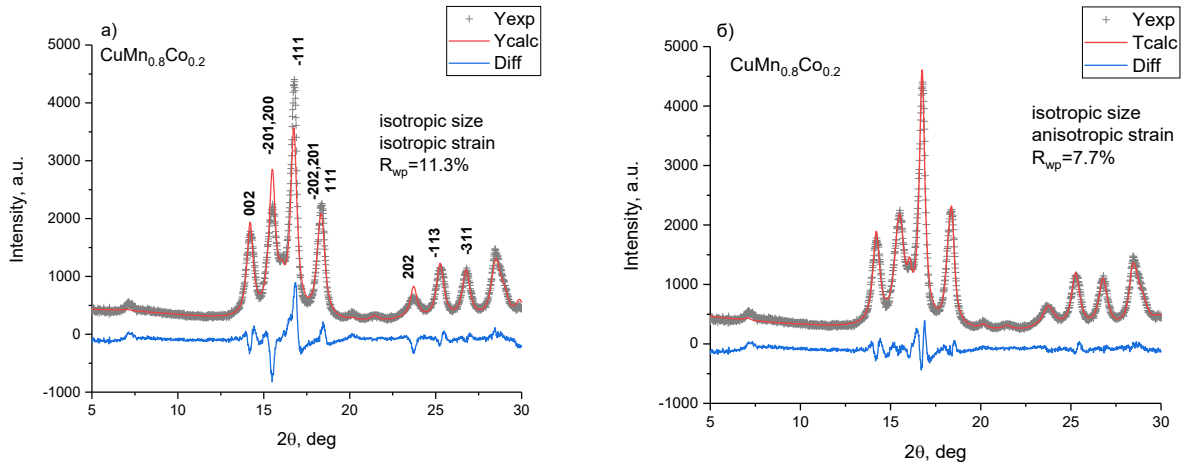


***Figure S2. Experimental (+) and simulated (red line) X-ray patterns for $CuMn_{0.8}Co_{0.2}$ as well as corresponding difference curve (blue line). The structure refinement was performed via the Rietveld method using (a) isotropic or (b) anisotropic models for microstrains simulation.***

***Fig.S2a*** shows experimental X-ray diffraction pattern for the $CuMn_{0.8}Co_{0.2}$ sample as well as the simulated Rietveld refinement based on the crednerite structure. Only the isotropic broadening of the diffraction lines (due to the change in the crystallite size and the concentration of microstrains) was taken into account for the refinement. In this case, the high value of $R_{wp}$ = 11.5 is due to a poor description of the experimental broadening for the reflections of -201, 200, 202 (not wide enough) and -111 (not narrow enough). Previously, the defect structure of the

$AgMnO_2$ oxide with a crednerite-type structure was discussed elsewhere [1]. The X-ray diffraction pattern of $AgMnO_2$ was also characterized by anisotropic broadening of the reflections, which was associated with the formation of planar defects. However, the presence of such defects in the crednerite structure causes a broadening of 110, -111, 111 reflections.

***Table S1. Phase composition and corresponding crystallite sizes in accordance with the full-profile Rietveld refinement of experimental X-ray patterns***

| Sample | Phases | As-prepared | | T=250°C | | T=350°C | |
|---|---|---|---|---|---|---|---|
| | | Content, wt.% | Crystal size, nm | Content, wt.% | Crystal size, nm | Content, wt.% | Crystal size, nm |
| CuMn | Crednerite $CuMnO_2$ | 100 | 39(6) | 100 | 19(2) | 25 | 15(1) |
| | Cubic spinel $(Cu,Mn)_3O_4$ | - | - | - | - | 73 | 14(2) |
| | Tenorite CuO | - | - | - | - | 2 | 12(2) |
| $CuMn_{0.9}Co_{0.1}$ | Crednerite $Cu(Mn,Co)O_2$ | 100 | 23(3) | 83 | 19(2) | - | - |
| | Cubic spinel $(Cu,Mn,Co)_3O_4$ | - | - | 17 | 11(2) | 95 | 11(1) |
| | Tenorite CuO | - | - | | | 5 | 9(1) |
| $CuMn_{0.8}Co_{0.2}$ | Crednerite $Cu(Mn,Co)O_2$ | 100 | 10(1) | 55 | 8(1) | - | - |
| | Cubic spinel $(Cu,Mn,Co)_3O_4$ | - | - | 45 | 7(1) | 93 | 10(1) |
| | Tenorite CuO | - | - | - | - | 7 | 7(1) |
| $CuMn_{0.7}Co_{0.3}$ | Crednerite $Cu(Mn,Co)O_2$ | 74 | 8(1) | 21 | 9(1) | - | - |
| | Tetragonal spinel $CoMn_2O_4$ | 18 | 7(1) | 18 | 6(1) | - | - |
| | Delafossite $CuCoO_2$ | 3 | ≈5* | 3 | ≈10* | 2 | 25(9) |
| | Tenorite CuO | 5 | 15(1) | 19 | 3.2(3) | 15 | 6.8(3) |
| | Cubic spinel $(Cu,Mn,Co)_3O_4$ | - | - | 38 | 3.9(1) | 83 | 13(1) |
| $CuMn_{0.5}Co_{0.5}$ | Cubic spinel $(Co,Mn)O_4$ | 71 | 4.9(2) | - | - | 65 | 11(1) |
| | Tenorite CuO | 12 | 20(1) | - | - | 27 | 32(6) |
| | Cuprite $Cu_2O$ | 17 | >100 | - | - | 8 | >100 |

**parameters were not refined due to low phase content;*

***Table S2. Structural parameters for crednerite particles in the composition of as-prepared $CuMn_{1-x}Co_x$ samples, where x=0, 0.1, 0.2, and 0.3***

| Sample | a, Å | b, Å | c, Å | β, ° | V, Å$^3$ | Microstrains* |
|---|---|---|---|---|---|---|

| | | | | | | |
|---|---|---|---|---|---|---|
| CuMn | 5.589(1) | 2.884(1) | 5.892(1) | 103.97(2) | 92.17(3) | 0.008(1) |
| $CuMn_{0.9}Co_{0.1}$ | 5.505(3) | 2.886(1) | 5.896(3) | 104.37(3) | 90.75(6) | 0.017(10 |
| $CuMn_{0.8}Co_{0.2}$ | 5.414(3) | 2.891(3) | 5.901(3) | 104.76(3) | 89.3(1) | 0.033(1) |
| $CuMn_{0.7}Co_{0.3}$ | 5.355(3) | 2.892(2) | 5.890(3) | 105.28(6) | 88.0(1) | ** |

** values averaged in all crystallographic directions;*
*** - parameters were not reliably obtained due to the presence of other interfering phases.*

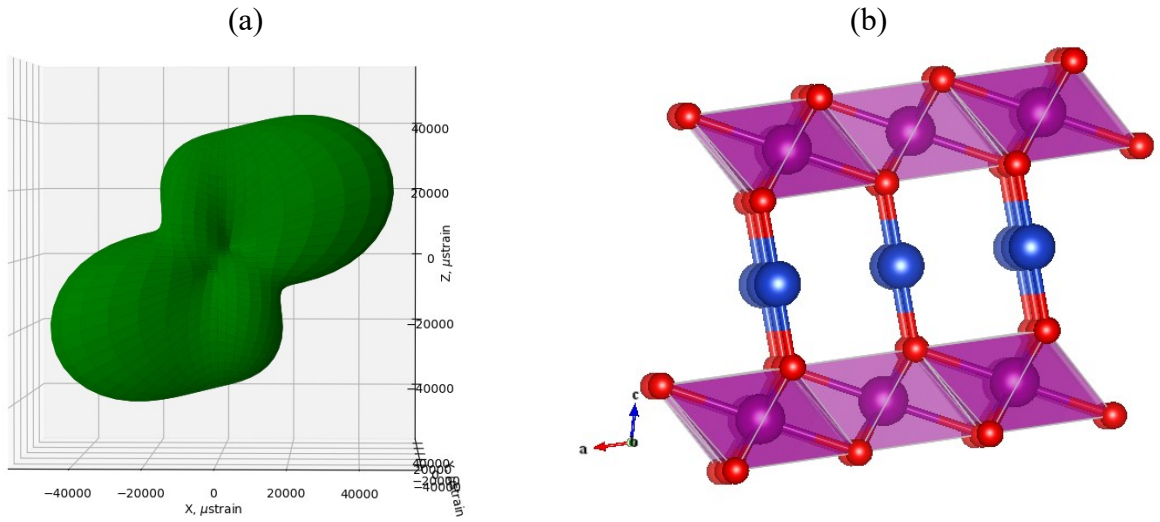


***Figure S3. (a) Graphic visualization of the refined elements of anisotropic microstrain tensor; (b) Crednerite structure in the xz plane reflecting the long Mn-O bonds of distorted octahedra $MnO_6$: blue circle – copper, red circle – oxygen, violet circle – manganese.***

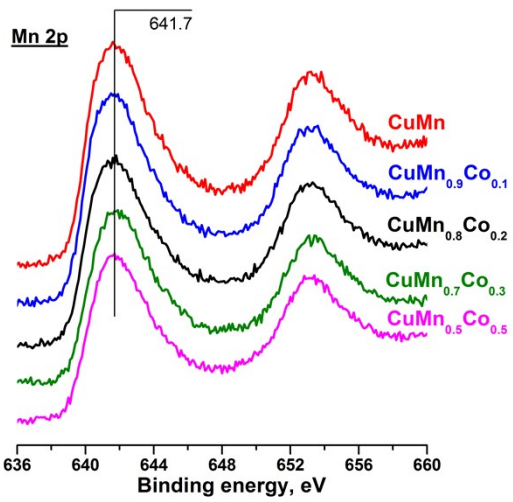


***Figure S4. Spectral regions of Mn 2p for as-prepared $CuMn_{1-x}Co_x$ catalysts with varied Co content (x=0, 0.1, 0.2, 0.3 u 0.5)***

***Table S3. The values of specific surface area according to the BET theory for studied catalysts***

| Sample | Specific surface area ($S_a$), $m^2/g$ |
|---|---|
| CuMn-250 | 35 |

| | |
|---|---|
| CuMn-350 | 32 |
| As-prepared $CuMn_{0.9}Co_{0.1}$ | 45 |
| $CuMn_{0.9}Co_{0.1}$-250 | 43 |
| $CuMn_{0.9}Co_{0.1}$-350 | 31 |
| As-prepared $CuMn_{0.8}Co_{0.2}$ | 54 |
| $CuMn_{0.8}Co_{0.2}$-250 | 46 |
| $CuMn_{0.8}Co_{0.2}$-350 | 37 |
| As-prepared $CuMn_{0.7}Co_{0.3}$ | 35 |
| $CuMn_{0.7}Co_{0.3}$-250 | 29 |
| $CuMn_{0.7}Co_{0.3}$-350 | 23 |
| As-prepared $CuMn_{0.5}Co_{0.5}$ | 52 |
| $CuMn_{0.5}Co_{0.5}$-350 | 49 |

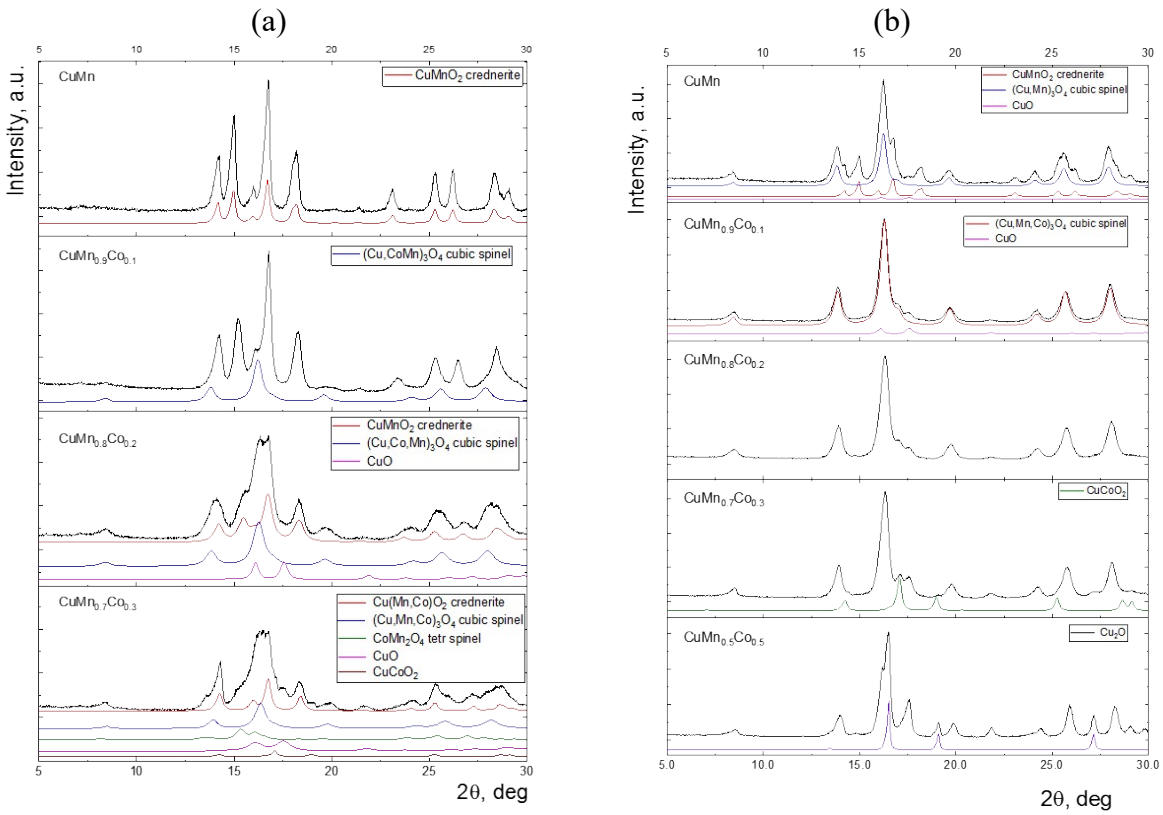


***Figure S5. Experimental X-ray patterns for $CuMn_{1-x}Co_x$ samples (x=0, 0.1, 0.2, 0.3 u 0.5) after catalytic measurements with heating up to (a) 250 and (b) 350°C in the comparison with simulated data for reference compounds. Simulation was performed using the full-profile Rietveld refinement. Quantitative data about phase composition and crystallite sized are presented in Table S1 above.***

***Table S4. Lattice and isotropic microstrain parameters for cubic spinel particles in the composition of $CuMn_{1-x}Co_x$ samples after catalytic measurements with heating up to 250 and 350°C***

| Sample | lattice parameter *a*, Å | | microstrains | |
|---|---|---|---|---|
| | T=250°C | T=350°C | T=250°C | T=350°C |
| CuMn | - | 8.303(1) | - | 0.24(2) |
| $CuMn_{0.9}Co_{0.1}$ | 8.320(6) | 8.280(2) | 0.41(6) | 0.26(2) |

| | | | | |
|---|---|---|---|---|
| $CuMn_{0.8}Co_{0.2}$ | 8.286(6) | 8.265(2) | 0.42(6) | 0.21(2) |
| $CuMn_{0.7}Co_{0.3}$ | 8.24(1) | 8.253(2) | -* | 0.24(1) |
| $CuMn_{0.5}Co_{0.5}$ | - | 8.205(2) | -* | 0.07(1) |

** - the parameter was not refined due to the presence of other interfering phases*

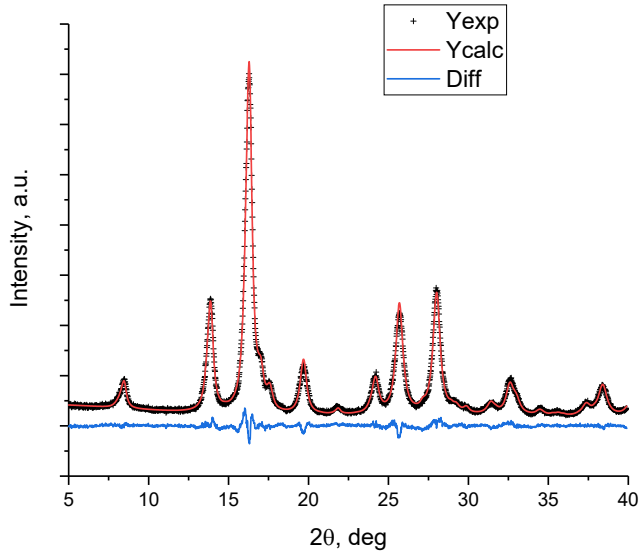


***Figure S6. Experimental (+) and simulated (red line) X-ray patterns for $CuMn_{0.8}Co_{0.2}$-350 sample as well as corresponding difference curve (blue line). Simulation was performed using the full-profile Rietveld refinement taking into the account the presence of both cubic spinel $(Cu,Mn,Co)_3O_4$ and CuO particles. In the case of spinel $(Cu,Mn,Co)_3O_4$ the model with Cu cations in both tetrahedral and octahedral positions was considered.***

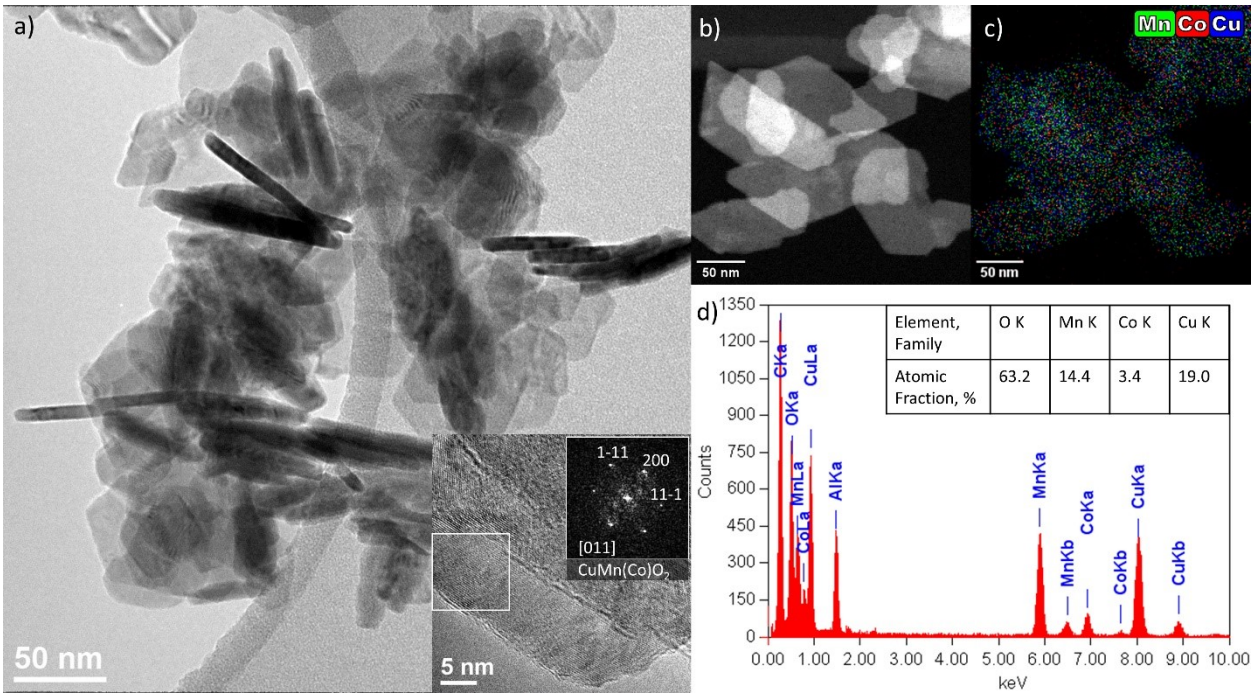

***Fig. S7. TEM data for $CuMn_{0.8}Co_{0.2}$ sample: (a) TEM image, high resolution TEM image and the insertion of FFT of selected area with indication of reflections from crednerite-type $CuMn(Co)O_2$ particles; (b) HAADF-STEM image and (c) corresponding EDX mapping showing the distribution of Mn (green), Co (red), and Cu (blue) in the sample as well as (d) corresponding EDX spectrum and quantitative data about element concentration for selected area.***

***Table S5. Quantitative TPR-CO data for CuMn and $CuMn_{0.8}Co_{0.2}$ samples after heating at 350°C in Ar or 20%$O_2$/Ar***

| | *CuMn | | *$CuMn_{0.8}Co_{0.2}$ | |
|---|---|---|---|---|
| | Ar | 20%$O_2$/Ar | Ar | 20%$O_2$/Ar |
| Evolved $CO_2$, 0-600°C | 6858 µmol/g | 12110 µmol/g | 6510 µmol/g | 12786 µmol/g |
| $CO/CO_2$, 0-600°C | 1.29 | 1.22 | 1.19 | 1.28 |
| Evolved $CO_2$, 0-100°C | 22 µmol/g | 127 µmol/g | 45 µmol/g | 204 µmol/g |
| δ for $CuMn_{1-x}Co_xO_{2+\delta}$ | - | 0.79 | - | 0.95 |
| $[O]_{100}/[O]_{600}$ | 0.003 | 0.0105 | 0.007 | 0.016 |

**total oxygen quantity for CuMn and $CuMn_{0.8}Co_{0.2}$ samples was calculated to be near 13291 and 13220 µmol/g respectively;*

***Table S6. Specific catalytic rates of dry CO oxidation over different hopcalites ($CuMnO_x$) at room temperature***

| $CuMnO_x$ synthesis | Reaction conditions | $GHSV_{CO}$, $ml \cdot h^{-1} \cdot g_{cat}^{-1}$ | Specific reaction rate $W_s$, $\times 10^{-3}$ $ml(CO) \cdot m^{-2} \cdot s^{-1}$ | $W_m$, $\times 10^{-2}$ $ml(CO) \cdot g^{-1} \cdot s^{-1}$ | Reference |
|---|---|---|---|---|---|
| Thermal decomposition of supercritically precipitated copper and manganese acetates | T=25°C<br>V=22.5 ml/min<br>$[CO]_0$=0.5 vol.%<br>$m_{cat}$=50 mg | 135 | - | **0.375** | S. Kondrat et al. [2] |
| Co-precipitation from copper and manganese nitrates using $Na_2CO_3$ | T=20°C<br>V=55 ml/min<br>$[CO]_0$=0.45 vol.%<br>$m_{cat}$=100 mg | 149 | 1.1 | **3.71** | G. Hutchings et al [3] |
| Co-precipitation from copper and manganese nitrates using $Na_2CO_3$ | T=25°C<br>V=21 ml/min<br>$[CO]_0$=0. 5 vol.%<br>$m_{cat}$=50 mg | 126 | 0.185 | **1.575** | T. Clarke, PhD thesis [4] |

| | | | | | |
|---|---|---|---|---|---|
| Co-precipitation from copper and manganese nitrates using $Na_2CO_3$ | T=25°C<br>V=22.5 ml/min<br>$[CO]_0$=0. 5 vol.%<br>$m_{cat}$=50 mg | 135 | 0.098 | **0.85** | C. Jones, PhD thesis [5] |

***Table S7. Specific catalytic rates of dry CO oxidation over various Cu-Co-Mn catalytic systems at near room temperature***

| Catalyst | Reaction conditions | $GHSV_{CO}$, $ml \cdot h^{-1} \cdot g_{cat}^{-1}$ | Specific reaction rate $W_s$, $\times 10^{-3}$ $ml(CO) \cdot m^{-2} \cdot s^{-1}$ | $W_m$, $\times 10^{-2}$ $ml(CO) \cdot g^{-1} \cdot s^{-1}$ | Reference |
|---|---|---|---|---|---|
| $CuMn_{0.8}Co_{0.2}$-350 | T=25°C<br>V=200 ml/min<br>$[CO]_0$=0.24 vol.%<br>$m_{cat}$=300 mg<br>S=37 $m^2/g$<br>light-off | 96 | **0.5** | 1.7 | This work |
| 1%Co/$CuMnO_x$ | T=25°C<br>V=22.5 ml/min<br>$[CO]_0$=0.5 vol.%<br>S=73 $m^2/g$<br>steady state (120 min) | 135 | **0.3** | 1.8 | C. Jones et al. [6] |
| Mn-Cu-Co | T=25°C<br>V=30 ml/min<br>$[CO]_0$=1 vol.%<br>$m_{cat}$=100 mg<br>S=176 $m^2/g$<br>light-off | 180 | **0.1** | 2.3 | K.-H. Choi et al. [7] |
| $CuMnCo_{RC3}$ | T=25°C<br>V=60 ml/min<br>$[CO]_0$=2.5 vol.%<br>$m_{cat}$=100 mg<br>S=138.6 $m^2/g$<br>light-off | 900 | **0.3** | 3.8 | S. Dey et al. [8] |
| $CoO_x$–$CuO_x$–10$MnO_x$ | T=30°C<br>V=83.33 ml/min<br>$[CO]_0$=5 vol.%<br>$m_{cat}$=900 mg<br>S=33.7 $m^2/g$<br>light-off | 278 | **1.3** | 4.2 | R.D. Kerkar et al [9] |
| Amorphous $CuCoMnO_4$ | **T=60°C**<br>V=60 ml/min<br>$[CO]_0$=1 vol.%<br>$m_{cat}$=20 mg<br>S=188 $m^2/g$<br>light-off | 1800 | **0.4** | 7.7 | P.A. Wright et al. [10] |
| Crystallized $CuCoMnO_4$ | **T=60°C**<br>V=60 ml/min<br>$[CO]_0$=1 vol.%<br>$m_{cat}$=20 mg<br>S=113 $m^2/g$<br>light-off | 1800 | **0.8** | 9.2 | P.A. Wright et al. [10] |
| CuO nanopowders | **T=65°C**<br>V=1000 ml/min<br>$[CO]_0$=0.2 vol.%<br>$m_{cat}$=188.5 mg<br>S=77 $m^2/g$<br>light-off | 637 | **0.23** | 1.8 | D.A. Svintsitskiy et al. [11] |

**References:**


[1] D.A. Svintsitskiy, V.M. Metalnikova, S. V. Cherepanova, A.I. Boronin, Appl. Catal. A Gen. 661 (2023) 119244.

[2] S.A. Kondrat, T.E. Davies, Z. Zu, P. Boldrin, J.K. Bartley, A.F. Carley, S.H. Taylor, M.J. Rosseinsky, G.J. Hutchings, J. Catal. 281 (2011) 279–289.

[3] G.J. Hutchings, A.A. Mirzaei, R.W. Joyner, M.R.H. Siddiqui, S.H. Taylor, Appl. Catal. A Gen. 166 (1998) 143–152.

[4] T.J. Clarke, Preparation of Copper Manganese Oxide Catalysts and Their Application for Oxidation Reactions, Cardiff University, 2015.

[5] C.D. Jones, Ambient Temperature Oxidation of Carbon Monoxide by Copper-Manganese Oxide Based Catalysts, Cardiff University, 2006.

[6] C. Jones, S.H. Taylor, A. Burrows, M.J. Crudace, C.J. Kiely, G.J. Hutchings, Chem. Commun. (2008) 1707–1709.

[7] K.H. Choi, D.H. Lee, H.S. Kim, Y.C. Yoon, C.S. Park, Y.H. Kim, Ind. Eng. Chem. Res. 55 (2016) 4443–4450.

[8] S. Dey, G.C. Dhal, D. Mohan, R. Prasad, R.N. Gupta, Appl. Surf. Sci. 441 (2018) 303–316.

[9] R.D. Kerkar, A. V. Salker, Appl. Nanosci. 11 (2021) 2861–2867.

[10] P.A. Wright, S. Natarajan, J.M. Thomas, P.L. Gai-Boyes, Chem. Mater. 4 (1992) 1053–1065.

[11] D.A. Svintsitskiy, A.P. Chupakhin, E.M. Slavinskaya, O.A. Stonkus, A.I. Stadnichenko, S.V. Koscheev, A.I. Boronin, J. Mol. Catal. A Chem. 368–369 (2013) 95–106.